aerospace

MDPI

Article

Orbit Determination of Cislunar Spacecraft Using Inter-Satellite Link Measurements with an Earth-Orbiting Satellite Constellation

Jiulong Liu [1,2,3,*], Jianfeng Sun [1,2,3,*], Qian Xu [1,2,3], Jiawen Shi [1,2,3] and Lidan He [1,2,3]

[1] Shanghai Satellite Network Research Institute Co., Ltd., Shanghai 201204, China; xuq2@chinasatnet.com.cn (Q.X.); shijw@chinasatnet.com.cn (J.S.); held@chinasatnet.com.cn (L.H.)
[2] Shanghai Key Laboratory of Satellite Network, Shanghai 201204, China
[3] State Key Laboratory of Satellite Network, Shanghai 201204, China
* Correspondence: liujl2@chinasatnet.com.cn (J.L.); sunjf@chinasatnet.com.cn (J.S.)

Abstract

With the increasing number of lunar missions, utilizing satellites in special orbits in the cislunar space as relay satellites to provide communication relay and navigation services for spacecraft near the Moon has become a hot topic. DRO (Distant Retrograde Orbit) and NRHO (Near-Rectilinear Halo Orbit) are widely used in lunar and deep space exploration missions, offering unique orbital advantages. With the development of a global constellation of LEO satellites, this paper utilizes intersatellite link measurements between LEO satellites and cislunar probes to determine orbital parameters. Under the adopted measurement-noise-only assumptions, Ka-band inter-satellite ranging yielded 3D position errors of 32.074 m for the DRO spacecraft and 20.665 m for the NRHO spacecraft. When laser ISL measurement accuracy reaches 10 times that of Ka-band measurements, simulations show positional accuracies of 2.206 m for NRHO satellite and 3.207 m for DRO satellite, respectively, representing an improvement of approximately 90%. The feasibility of orbit determination for cislunar spacecrafts based on intersatellite link measurements between LEO satellite constellation and cislunar spacecrafts has been verified through simulations. In the future, LEO satellite constellations could play a greater role in cislunar space exploration and even deep space exploration.

Keywords: orbit determination; deep space exploration; intersatellite link measurement; low earth orbit satellite constellations; cislunar navigation

Check for updates

Academic Editor: George Z. H. Zhu

Received: 30 July 2026
Revised: 16 September 2026
Accepted: 23 September 2026
Published: 25 September 2026

Copyright: © 2026 by the authors. Licensee MDPI, Basel, Switzerland. This article is an open access article distributed under the terms and conditions of the Creative Commons Attribution (CC BY) license.

1. Introduction

Over the past 15 years, we have witnessed a resurgence in lunar exploration, with several countries resuming or launching lunar exploration programs. China's lunar and deep space exploration began with the Chang'e-1 lunar probe, launched in 2007 [1]. From 2010 to 2024, Chang'e-2–6 missions were launched, carrying out multiple missions, including mapping the lunar surface, soft landing, lunar surface exploration, and sample return from the front and back of the moon [2–7]. Concurrently, the Queqiao-1 and Queqiao-2 relay communications satellites were launched to support lunar exploration missions [8]. The United States launched GRAIL in 2011 to study the lunar gravity field [9]; LADEE in 2013 to study the lunar atmosphere and dust [10]; Artemis-1 in 2022 to demonstrate unmanned spacecraft [11]; and CAPSTONE in 2022 to demonstrate cislunar navigation technology [12]. Over the next 15 years, both China and the United States have formulated

even more ambitious lunar exploration plans, encompassing manned missions, exploration and development of resources at the lunar south pole, and the construction of a lunar research station.

To ensure the success of lunar exploration and even deep space exploration missions, it is necessary to determine the spacecraft's orbit and determine its position and velocity in space. At present, lunar spacecraft orbit determination primarily relies on ground-based radiometric tracking, including techniques such as radio ranging, Doppler measurements, VLBI measurements, and ΔDOR measurements. In practice, these techniques are often combined to achieve higher orbit determination accuracy. In 2009, NASA launched the LRO. The primary radiometric tracking facility for LRO was the NASA White Sands ground station (WS1), which typically tracked the spacecraft for 8–10 h per day. The overall root-mean-square (RMS) value of the S-band Doppler range-rate residuals at WS1 was approximately 0.2 mm/s. Following hardware improvements, the RMS decreased from 0.22 mm/s before August 2012 to 0.13 mm/s thereafter [13]. The initial orbit determination accuracy requirement was 50 m. radio tracking and the LOLA data enabled an accuracy of approximately 20 m [13]. China has established the CDSN and the VLBI network, a ground-based deep space tracking and control system, to support orbit determination for lunar and even deep space probes. For example, in the 2024 Chang'e-6 lunar probe orbit determination mission, ranging and VLBI data were used to improve the orbit accuracy of the 160 km × 2400 km elliptical orbit from 145 m to 17 m, and the orbit accuracy of the 180 km × 230 km near-circular orbit from 100 m to 45 m [14].

While ground-based tracking networks have played a vital role in deep space exploration, their limitations are being exposed as lunar and even deep space exploration missions increase. While ground-based tracking networks offer global coverage, geographical and political constraints result in uneven distribution of stations. Furthermore, ground-based tracking networks require coordination of ground station resources, and their establishment and maintenance are costly. As the number of lunar missions increases, the capacity of the ground-based radio tracking network may be unable to meet demand, potentially leading to bottlenecks.

Using satellites in special orbits in the Earth–Moon space as relay satellites to provide communication relay and navigation services for spacecraft near the Moon has become a hot research topic [15]. The motion of spacecraft in cislunar space is commonly analyzed initially using the circular restricted three-body problem (CR3BP), an idealized model in which the Earth and Moon move in circular orbits about their common barycenter and the spacecraft is assumed to have negligible mass. Within this framework, a distant retrograde orbit (DRO) belongs to a family of large lunar-centered periodic orbits that appear retrograde in the Earth–Moon rotating reference frame. Many members of this family exhibit favorable long-term stability [16,17]. A near-rectilinear halo orbit (NRHO), by contrast, is a highly elongated three-dimensional member of the halo-orbit families associated with the Earth–Moon L1 or L2 collinear libration points. An NRHO alternates between a relatively close lunar passage and a distant excursion from the Moon [18–20]. Because DROs and NRHOs have distinctly different geometries and dynamical characteristics, they are selected in this study as two representative cislunar orbit cases.

In 2024, China launched the DRO lunar exploration mission. The three satellites, DRO-A, DRO-B, and DRO-L, were launched in succession, forming the world's first three-satellite constellation of the Earth–Moon system. The mission explored the use of LEO satellites to assist lunar probes in orbit determination. The DRO lunar probe uses the ground-based deep space network and the VLBI network to achieve an orbit determination accuracy of hundreds of meters and a velocity accuracy better than 0.4 cm/s [21]. DRO-A and DRO-B establish inter-satellite ranging links with DRO-L, achieving continuous measurement

through K-band microwave communication and estimating orbital states using the EKF method. Using the same-beam differential relative navigation method, simulations have shown a relative navigation position accuracy of 5 m [22].

An inter-satellite link (ISL) is a direct radio-frequency or optical link established between two spacecraft. In addition to transferring communication data, an ISL can generate one-way or dual one-way pseudorange measurements from the signal propagation time, thereby providing observations for orbit determination and time synchronization [23,24]. The BeiDou Navigation Satellite System (BDS-3) has demonstrated Ka-band ISL ranging and its application to satellite orbit determination and clock estimation [23,24]. In the present study, an ISL specifically denotes a Ka-band microwave or laser ranging link established between a LEO satellite and a cislunar spacecraft. The inter-satellite link ranging accuracy of BDS-3 satellites can reach 10 cm [23]. The radial overlap difference between the autonomous orbits of IGSO satellites is less than 15.0 cm, and the radial overlap difference between the autonomous orbits of MEO satellites is less than 10.0 cm [24]. Establishing ISLs between navigation satellites and lunar satellites can improve the accuracy of autonomous orbit determination of the navigation system [25]. Taking a hybrid constellation consisting of libration point probes, DRO probes and MEO satellites as a typical scenario, the autonomous orbit determination accuracy of the cislunar space probe based on inter-satellite ranging can be better than 10 m under the condition of 1 m ranging error [26]. Based on DRO-LLO satellite surface tracking and lunar laser ranging, the position accuracy of DRO satellite can reach 10 m [27]. The orbital parameters and performance characteristics mentioned in the references are listed in Table 1 below.

Table 1. Orbit configurations and definitions of representative performance values reported in previous studies.

Ref.	Orbit Configuration and Key Descriptors	Measurement and Estimation Setting	Reported Performance
[21]	Earth–Moon DRO reference trajectory from 29 November 2021 to 25 January 2022, represented in the Earth–Moon rotating frame	2-day OD arcs; 2 h of ranging per day plus one 2 h VLBI session; range and VLBI-delay noise of 3.0 and 0.3 m, respectively	Mean position RMS: 200.6 m; mean velocity RMS: 0.39 cm/s
[22]	DRO approximately 4.0×10^5 km from Earth and 7.0–10.0 $\times 10^4$ km from the Moon; period $\approx$ 14 d; 500 km sun-synchronous LEO, period $\approx$ 1.5 h; inter-DRO separations of approximately 50 km and $O(10^4)$ km	Same-beam differential satellite-to-satellite tracking; range-noise RMS $\approx$ 0.5 m	4.09 and 5.05 m
[23]	Five BDS-3 experimental spacecraft: two IGSO and three MEO spacecraft; nominal $h_{IGSO} \approx$ 35,786 km, $i_{IGSO} \approx 55^\circ$; $h_{MEO} \approx$ 21,528 km, $i_{MEO} \approx 55^\circ$	In-orbit Ka-band ISL measurements	$\leq$10 cm
[24]	Four BDS-3 experimental spacecraft in IGSO and MEO	Centralized autonomous OD using ISL measurements	<15 cm for IGSO and <10 cm for MEO
[26]	Earth–Moon L1/L2/L4/L5 spacecraft, one DRO spacecraft, and one MEO spacecraft; epoch: 30 September 2016, 00:00 UTC; MEO $a \approx$ 27,906 km and $i \approx 55^\circ$	7-day arc; 1 m ISL range noise; MEO position constrained to an accuracy of 1 m	Cislunar 3D position errors of 1.993–7.216 m; DRO: 2.229 m
[27]	One Earth–Moon DRO spacecraft and one LLO spacecraft at an altitude of 300 km	DRO–LLO satellite-to-satellite ranging combined with LLO-to-lunar-surface laser ranging	DRO: approximately 10 m; LLO: approximately 0.1 m

Note: h, i and a denote nominal altitude, inclination, and semimajor axis, respectively. Nominal BDS orbital parameters are provided to identify the orbit classes; the actual osculating elements depend on the spacecraft and epoch.

With the construction of global LEO satellite constellations, the manufacturing and launch costs of LEO satellites are gradually decreasing. Therefore, it is possible to explore the use of LEO constellations and ISL measurement technology (including microwave and laser links) to determine the orbit of lunar spacecrafts. This Article aims to demonstrate the feasibility of a lunar satellite orbit determination method based on ISL measurements of a LEO satellite constellation. We simulated a LEO satellite constellation and, using ISL measurement techniques (including microwave and laser), simulated orbit determination for satellites in both DRO and NRHO lunar orbits. We then analyzed the feasibility and effectiveness of this method.

2. Materials and Methods

This paper uses Ka-band and laser ISL measurements with cislunar satellites and LEO satellite constellation as observational variables to determine the orbits of cislunar satellites. The positions and event times of the transmitting and receiving spacecraft must be represented in a consistent coordinate and time framework before the inter-satellite range is calculated. The Barycentric Celestial Reference System (BCRS) is a relativistic celestial reference system centered at the solar-system barycenter, whereas the Geocentric Celestial Reference System (GCRS) is centered at the Earth's center of mass. In the present implementation, Terrestrial Time (TT) and Barycentric Dynamical Time (TDB) are used as the time arguments for the geocentric orbit calculations and barycentric ephemeris calculations, respectively. The LEO satellite states and observation epochs are transformed consistently from the geocentric framework to the barycentric framework before evaluating the cislunar light-time equation. The coordinate and time transformations follow the IERS Conventions (2010) [28]. This is the time variable in the satellite equations of motion established in the GCRS and BCRS. Only after unifying the time and coordinate systems into a consistent time and coordinate framework can high-precision modeling of the measurement model be guaranteed [26]. This paper aims to perform simulation verification, so appropriate simplifications are made based on the high-precision model.

2.1. Simplified ISL Ranging Measurement Model

Following the dual one-way ISL measurement architecture used by BDS-3 [24,29], a time division multiple access (TDMA) scheme is adopted. TDMA allows multiple satellite terminals to share the available link resources by assigning non-overlapping transmission and ranging time slots to different satellite pairs. For a scheduled pair of satellites i and j, satellite i transmits a ranging signal to satellite j, and satellite j transmits a signal in the opposite direction during another assigned time slot. The resulting two one-way pseudorange observations, acquired at different epochs t_1 and t_2, constitute a dual one-way measurement. Using the predicted satellite orbits and clock information, the two observations are transferred to a common epoch t_k before the geometric range is derived [24]. In the constellation simulation conducted in this study, one visible LEO satellite is selected to track the cislunar spacecraft during each 30 min tracking interval, after which the active link may be handed over to another visible LEO satellite.

As shown in Figure 1, a pair of satellites i and j receive pseudorange measurements from each other at different times, generating pseudorange observations $\rho_{ij}(t_1)$ and $\rho_{ji}(t_2)$ at times t_1 and t_2, respectively. Tang et al. [24] used the predicted satellite orbits and clock information to transform the observations at times t_1 and t_2 to a common time t_k. The observation equation can be expressed as:

$$\frac{\rho_{ij}(t_k) + \rho_{ji}(t_k)}{2} = \left|\vec{R}_j(t_k) - \vec{R}_i(t_k)\right| + c \times X^i_{Delay} + c \times X^j_{Delay} + \frac{\Delta\rho^{ij}_{cor} + \Delta\rho^{ji}_{cor}}{2} + \varepsilon \quad (1)$$

where $\vec{R_i}$ and $\vec{R_j}$ represent the Cartesian coordinate vectors of satellites i and j, respectively; $X^i_{Delay} = \frac{\tau_i^{\text{Transmit}} + \tau_i^{Rcv}}{2}$, ($X^j_{Delay} = \frac{\tau_j^{\text{Transmit}} + \tau_j^{Rcv}}{2}$), with $\tau_i^{\text{Transmit}}\left(\tau_j^{\text{Transmit}}\right)$ and $\tau_i^{Rcv}\left(\tau_j^{Rcv}\right)$ representing the hardware transmit and receive delays of satellite i(j), respectively; $\Delta\rho^{ij}_{cor}$ and $\Delta\rho^{ji}_{cor}$ represent model corrections for the two ranging measurements, including corrections for detector antenna phase center, ionospheric effects, and gravitational time delay; ε accounts for observation noise and other unknown systematic errors.

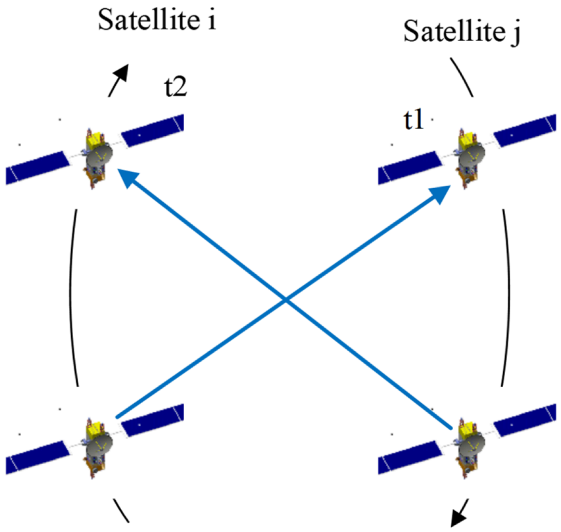


Figure 1. Time division multiple access inter-satellite link. The black arrows indicate the direction of satellite motion, while the blue arrows indicate the direction in which inter-satellite links are established.

Since the simulations in this paper do not consider satellite clock errors, orbit determination can be performed using Formula (1).

2.2. Precise Orbit Determination

According to Huang et al. [26], assume that at epoch t_k, spacecraft i performs a ranging measurement with spacecraft j. R is the geometric distance between spacecraft i and j (ignoring light-time effects for simplicity):

$$R_{ij} = R_{ji} = R = \sqrt{(x_i - x_j)^2 + (y_i - y_j)^2 + (z_i - z_j)^2} \tag{2}$$

where (x_i, y_i, z_i) and (x_j, y_j, z_j) are the three-dimensional coordinates of spacecraft i and j, respectively. Linearizing the intersatellite link observation equation at time t_k yields the following observation equation:

$$\boldsymbol{y}_k = \boldsymbol{H}_k \boldsymbol{x}_0 + \boldsymbol{\varepsilon}_k \tag{3}$$

where the measurement error $\boldsymbol{\varepsilon}_k = (\boldsymbol{\varepsilon}_{ij} + \boldsymbol{\varepsilon}_{ji})/2$; $\boldsymbol{y}_k$ in the observation equation is the observation residual $(m \times 1)$; $\boldsymbol{H}_k$ is the coefficient matrix $(m \times n)$, where m is the number of intersatellite link observations, n is the number of parameters to be solved, and $\boldsymbol{x}_0$ is the parameter to be solved. The partial derivative of the observation with respect to the satellite position can be divided into two parts:

$$\begin{gathered} \boldsymbol{H}_k = \left(\frac{\partial r_{ij}}{\partial(X_i, X_j)}\right)_{t_k} \frac{\partial(X_i, X_j)}{\partial(X^0{}_i, X^0{}_j)} = \left(\frac{\partial r_{ij}}{\partial(X_i, X_j)}\right)^*_{t_k} \Phi(t_k, t_0) \\ \dot{\Phi}(t, t_0) = A(t)\Phi(t, t_0),\ \Phi(t_0, t_0) = I \end{gathered} \tag{4}$$

The first part of the partial derivative above can be expressed as follows, and the second part is obtained by integration.

$$\left(\frac{\partial r_{ij}}{\partial(X_i, X_j)}\right)^*_{t_k} = \left(\frac{x_i - x_j}{R}, \frac{y_i - y_j}{R}, \frac{z_i - z_j}{R}, 0, 0, 0, -\frac{x_i - x_j}{R}, -\frac{y_i - y_j}{R}, -\frac{z_i - z_j}{R}, 0, 0, 0\right) \quad (5)$$

The least squares solution to the observation equation is as follows, where P is the observation weight matrix,

$$\boldsymbol{x} = \left(\boldsymbol{H}^T \boldsymbol{P} \boldsymbol{H}\right)^{-1} \left(\boldsymbol{H}^T \boldsymbol{P} \boldsymbol{y}\right) \quad (6)$$

3. Results

3.1. Simulation Scenario

The simulation conditions used in this paper, as well as the orbital information of the LEO constellation and the cislunar spacecrafts, are shown in Table 2 below. The initial epoch is 00:00 UTC on 19 June 2026, and the simulation duration is 7 days. Coordinates are based on the J2000.0 ECI coordinate system. Since this paper primarily analyzes the feasibility of orbit determination for cislunar spacecrafts using ISL measurements from a LEO satellite constellation, to isolate the effects of errors, only random measurement errors are considered for now, ignoring other dynamic model errors. Based on empirical experience with ISL accuracy, the ranging accuracy of the microwave (Ka-band) ISLs between the LEO satellite and the cislunar spacecraft is set to 1.0 m, and the ranging accuracy of the laser ISLs is set to 0.1 m.

Table 2. Simulation conditions of the POD using ISLs data.

Measurement Data Type	Measurement Error	Sampling Rate (Epoch Interval)
Ka-band ISL Ranging	Random Error: 1.0 m	5 min
Laser ISL Ranging	Random Error: 0.1 m	5 min

The LEO satellite constellation is generated by the LEO information in Table 3 below. The supporting constellation used in this study is an idealized Walker-Delta LEO constellation rather than an existing operational constellation. It is defined using the Walker notation i:$T/P/F$ = 60°:32/8/1 , where $T = 32$ is the total number of satellites, $P = 8$ is the number of orbital planes, and $F = 1$ defines the relative phasing between adjacent planes. Each orbital plane contains four satellites in nominally circular orbits at an altitude of 500 km, corresponding to a semi-major axis of approximately 6878.14 km. The orbital planes span 360° in RAAN, with an adjacent-plane RAAN separation of 45°. Satellites within each plane are separated by 90° in argument of latitude. All constellation states are expressed in the J2000.0 ECI frame. During the orbit-determination simulations, the LEO satellite ephemerides are treated as fixed and error-free.

Table 3. Initial orbit information in the POD simulation with ISLs data.

Spacecraft/Satellite	X (m)	Y (m)	Z (m)	VX (m/s)	VY (m/s)	VZ (m/s)
NRHO	−287,650,887.3	210,466,587.6	104,551,177.1	38.052	213.127	−187.494
DRO	−359,201,791.8	221,223,869.0	88,726,233.7	−590.746	−424.941	−311.212
LEO	6,862,990.301	227,891.370	395,271.427	−504.981	3797.937	6578.179

3.2. Establishment Status

The following Figures 2 and 3 show the visibility of LEO constellation satellites and the target satellite. The following Table 4 shows the number of visible satellites between the target satellite and the LEO satellites and the number of link establishment epochs:

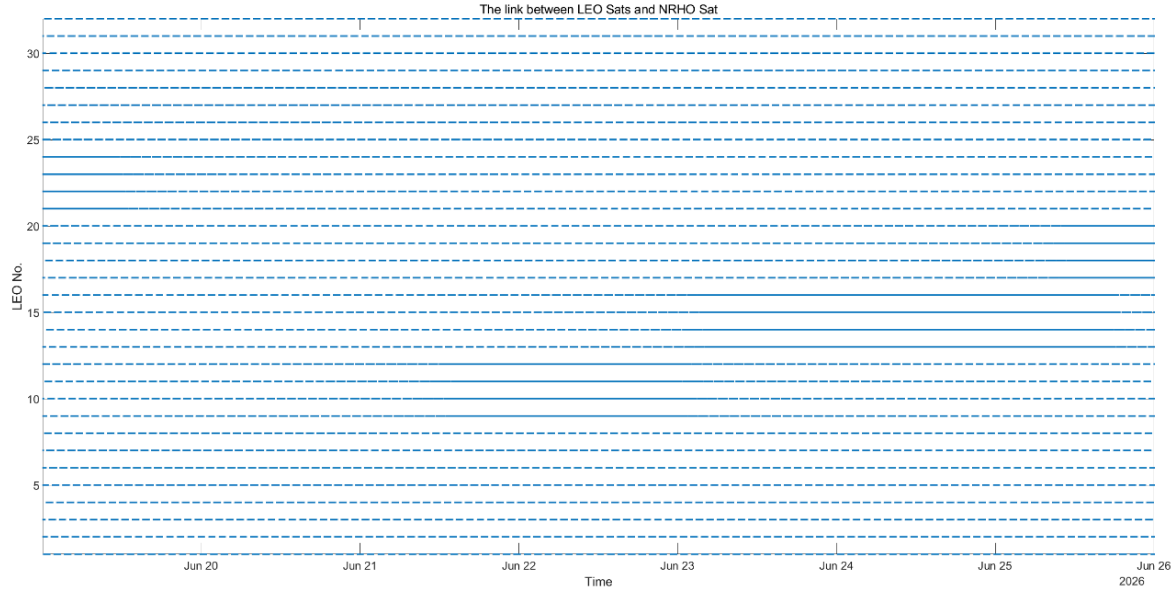


Figure 2. Link establishment status of LEO satellites and NRHO satellite (The horizontal axis represents the epoch number, while the vertical axis represents the satellite index in the LEO constellation. Each blue dot indicates that the target satellite and the LEO satellite are mutually visible at that epoch, allowing an ISL to be established.).

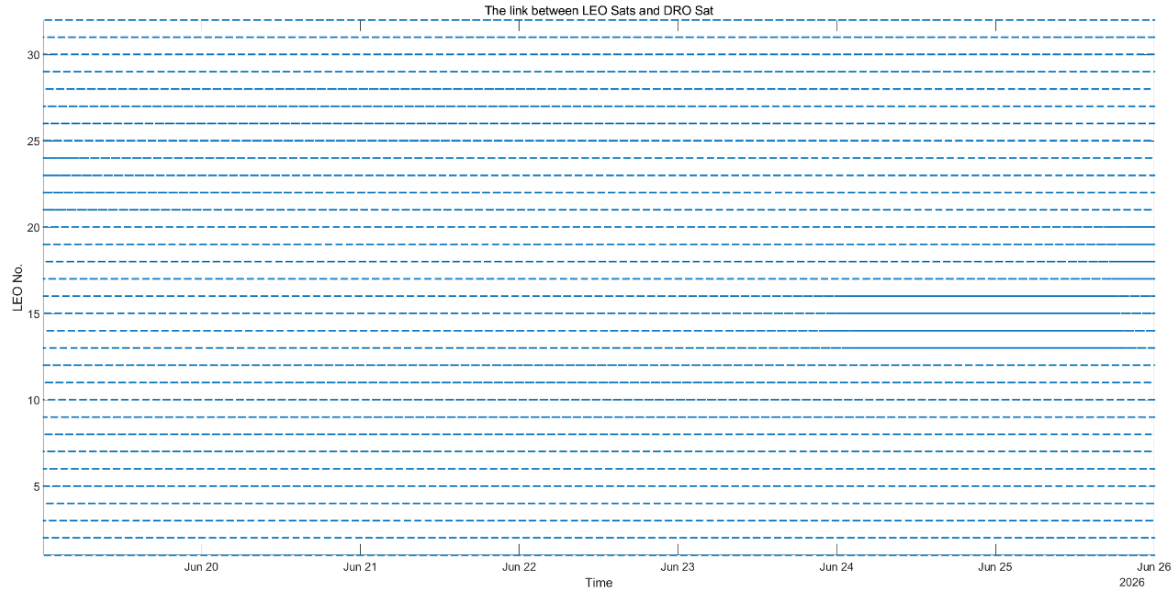


Figure 3. Link establishment status of LEO satellites and DRO satellite (The horizontal axis represents the epoch number, while the vertical axis represents the satellite index in the LEO constellation. Each blue dot indicates that the target satellite and the LEO satellite are mutually visible at that epoch, allowing an ISL to be established.).

Table 4. Statistics of the number of visible satellites and link establishment epochs between the target satellites and LEO satellites.

Target Satellite	Number of Visible Satellites			Average Number of Continuous Link Establishment Epochs
	Minimum	Maximum	Average	
NRHO	19	26	22.0	14.5
DRO	19	26	21.6	13.3

Considering that in actual missions, the target satellite will not establish links with multiple satellites simultaneously. Also, considering that in actual application scenarios, if the target satellite frequently switches links, it will increase the difficulty of operating the control system, here, based on the link establishment situation, within a time period (30–40 min), the target satellite maintains a stable link with any continuously visible satellite in the LEO satellite constellation.

3.3. The Results of POD

The simulation uses the J2000.0 ECI as the reference system. The precession/nutation model recommended by IERS 2010 is used during the simulation and POD process, and the EOP model uses the EOP product released by IERS. For LEO satellites, the JGM120*120 Earth gravity field model is used, while for cis-lunar probes, the JGM40*40 Earth gravity field model is used. Furthermore, the N-body gravity model uses the JPL DE405 ephemeris, and the IERS 2010 model is used for Earth tidal perturbations. For parameter estimation, POD employs a least-squares batch method. The orbit determination arc length is 7 days, and the integration step for the cis-lunar probe is 60 s. The LEO satellite's orbit is also fixed.

The following Figures 4 and 5 show the position-error time series for the NRHO and DRO spacecraft. In each panel, the purple curve denotes the three-dimensional position-error magnitude, $e_{3D} = \sqrt{e_X^2 + e_Y^2 + e_Z^2}$, whereas the blue, orange, and yellow curves denote the signed position errors in the X, Y, and Z directions, respectively. Panels (a) and (b) present the results obtained using Ka-band and laser ISL ranging, respectively.

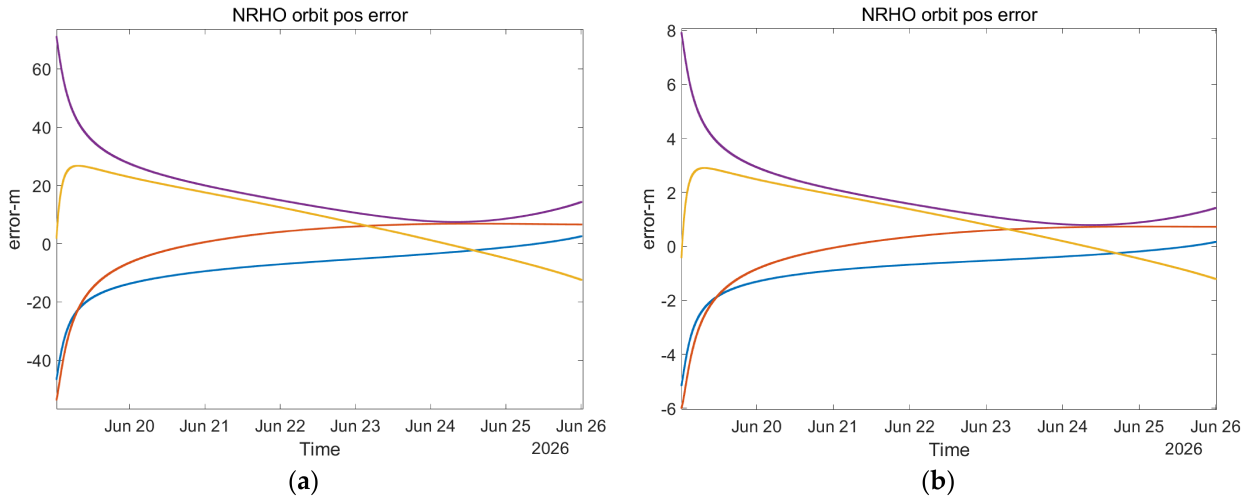


Figure 4. Position-error time series for the NRHO spacecraft obtained using (**a**) Ka-band ISL ranging and (**b**) laser ISL ranging. The purple curve represents the three-dimensional position-error magnitude, while the blue, orange, and yellow curves represent the signed X-, Y-, and Z-component errors, respectively.

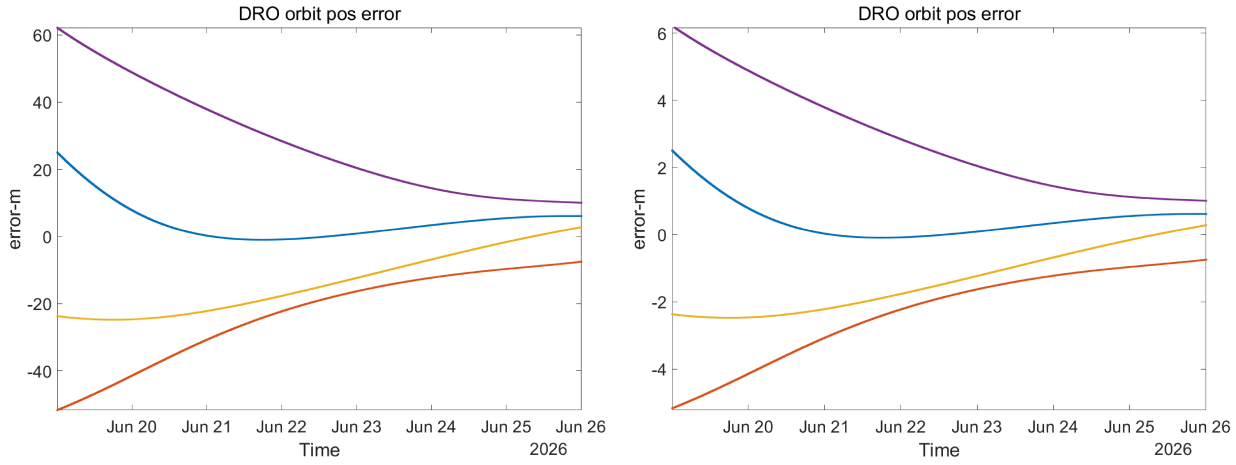


Figure 5. Position-error time series for the DRO spacecraft obtained using (**a**) Ka-band ISL ranging and (**b**) laser ISL ranging. The purple curve represents the three-dimensional position-error magnitude, while the blue, orange, and yellow curves represent the signed X-, Y-, and Z-component errors, respectively.

Using ISL measurements of the LEO satellite constellation, the orbit determination results of NRHO satellite and DRO satellite are summarized in the following Table 5:

Table 5. Statistics of orbit determination results.

Measurement Mode	Satellite	Position Error (m)				Speed Error (mm/s)			
		X	Y	Z	3D	VX	VY	VZ	3D
Ka-band ISL Ranging	NRHO	10.813	10.348	14.249	20.665	0.24	0.29	0.48	0.62
	DRO	7.059	26.586	16.496	32.074	0.09	0.08	0.05	0.13
Laser ISL Ranging	NRHO	1.086	1.144	1.543	2.206	0.03	0.03	0.05	0.07
	DRO	0.706	2.659	1.650	3.207	0.01	0.01	0.01	0.02

4. Discussion

A simulation generated a 32-LEO satellite constellation (8 orbital planes, 4 satellites per plane) with an orbital altitude of 500 km and an orbital inclination of 60 degrees. Approximately 20 satellites in the constellation were visible to the target satellites (DRO and NRHO satellites) during each observation epoch, with an average visibility duration of approximately 60 min. A LEO satellite that could establish a link with the target satellite was selected for continuous observation for 30 min, after which another LEO satellite was switched to establish a link with the target satellite to improve the observation geometry.

Based on the Ka-band ISL measurements with an assumed ranging error of 1.0 m, the 3D position errors of the NRHO and DRO spacecraft were 20.665 and 32.074 m, respectively, while the corresponding 3D velocity errors were 0.62 and 0.13 mm/s. With the laser ISL ranging error set to 0.1 m, the 3D position errors decreased to 2.206 m for the NRHO spacecraft and 3.207 m for the DRO spacecraft.

For context, Ref. [21] reported ground-based DRO orbit-determination errors at the kilometer-to-hundreds-of-meters level, depending on the observation-arc length and whether ranging measurements were combined with VLBI data. However, those results are not directly comparable with the present ISL-only results. In Ref. [21], the hundreds-of-meters result was obtained from a two-day short-arc solution combining ground-based ranging and VLBI observations, whereas the present result was obtained from a seven-day ISL arc with a 5 min sampling interval. Moreover, the present simulation considers only

random ranging errors and treats the LEO satellite orbits as fixed. The two studies also differ in observation geometry, data coverage, measurement types, dynamical modeling, and error assumptions. Consequently, the numerical difference between the reported results cannot be attributed solely to the use of ISL rather than ground-based measurements.

Under the common seven-day observation arc, the Ka-band and laser ISL simulations used the same sampling interval, link schedule, dynamical model, and batch least-squares estimator. The only difference was the standard deviation of the assumed random ranging error, which was reduced from 1.0 m for the Ka-band measurements to 0.1 m for the laser measurements. For a batch least-squares solution, the formal state covariance is approximately $C_{\hat{x}} = \left(H^{\mathrm{T}} R^{-1} H\right)^{-1}$. Because the coefficient matrix H is unchanged and the laser measurement-noise covariance satisfies $R_{\mathrm{laser}} = 0.01 R_{\mathrm{Ka}}$, the formal standard deviations of the estimated state are expected to decrease by approximately a factor of 10. Consistent with this relationship, the 3D position error decreased from 20.665 to 2.206 m for the NRHO case and from 32.074 to 3.207 m for the DRO case, corresponding to reductions of 89.3% and 90.0%, respectively. The approximately proportional reduction therefore results primarily from the measurement-noise-limited configuration of the present simulations.

Although the relative reductions are similar, the two orbital cases exhibit different absolute errors and component-wise error distributions. For the DRO, the Y-component position error is substantially larger than the X- and Z-component errors: it decreases from 26.586 m for the Ka-band solution to 2.659 m for the laser solution. By comparison, the NRHO position errors are more evenly distributed among the three coordinate components. Because an inter-satellite range measurement primarily constrains the spacecraft state along the instantaneous line of sight, the distinct line-of-sight histories and state-transition matrices of the DRO and NRHO produce different component-wise observability over the seven-day arc. The different orbit-determination results should be interpreted in terms of both measurement geometry and dynamical sensitivity. At the initial epoch of 19 June 2026, 00:00 UTC, the Moon-centered distances of the NRHO and DRO spacecraft are approximately 6743 and 71,621 km, respectively. The NRHO spacecraft therefore initially experiences a substantially stronger lunar gravity gradient. An auxiliary seven-day propagation using an Earth–Moon–Sun point-mass model shows substantially larger variations in Moon-centered distance and more pronounced out-of-plane motion for NRHO. These differences affect both the line-of-sight history and the state-transition matrix, potentially providing more diverse constraints on the estimated state. This interpretation is consistent with the smaller NRHO position error reported in Table 5. The laser measurements reduce the magnitude of the measurement noise but do not alter this underlying observation geometry. Consequently, they produce nearly the same relative improvement for both orbits while preserving their different error distributions.

These results should be interpreted as a sensitivity assessment under idealized conditions rather than as evidence that laser ISLs universally improve orbit-determination accuracy by 90%. The simulations include only random ranging errors and treat the LEO satellite orbits as fixed. In an operational system, ephemeris and clock errors, ranging biases, dynamical-model errors, link interruptions, and laser pointing and acquisition constraints may introduce an accuracy floor, causing the improvement to deviate from the proportional relationship observed here.

5. Conclusions

For cislunar space exploration, orbital parameters can be calculated using ISL measurements with LEO satellite constellations. Under the adopted simulation assumptions, the Ka-band ISL measurements yielded 3D position errors of 32.074 m for the DRO spacecraft and 20.665 m for the NRHO spacecraft. Under the idealized measurement-noise-only

assumptions, reducing the ranging-error standard deviation from 1.0 m for the Ka-band ISLs to 0.1 m for the laser ISLs reduced the 3D position errors of the NRHO and DRO spacecraft by 89.3% and 90.0%, respectively. This near-proportional improvement represents a measurement-noise-limited simulation result and should not be interpreted as a universal performance gain of laser ISLs under operational conditions.

The simulation validates the feasibility of POD for cislunar spacecraft based on ISL measurements between LEO satellite constellations and spacecrafts. In the future, LEO satellite constellations could play a greater role in cislunar space exploration and even deep space exploration.

Author Contributions: Conceptualization, J.L. and J.S. (Jianfeng Sun); Methodology, J.L.; Software, J.L.; Validation, J.L.; Formal analysis, J.L. and J.S. (Jiawen Shi); Investigation, J.L.; Resources, J.L.; Data curation, J.L. and J.S. (Jiawen Shi); Writing—original draft, J.L.; Writing—review and editing, J.S. (Jianfeng Sun) and Q.X.; Visualization, J.L.; Supervision, J.S. (Jianfeng Sun), Q.X. and L.H.; Project administration, Q.X., J.S. (Jiawen Shi) and L.H.; Funding acquisition, J.S. (Jianfeng Sun) and L.H. All authors have read and agreed to the published version of the manuscript.

Funding: This work is supported by Mobile Information Networks-National Science and Technology Major Project under Grant no. 2025ZD1302900.

Data Availability Statement: The data that support the findings of this study are available from the corresponding author upon reasonable request.

Acknowledgments: We would like to thank Yanling Chen from Shanghai Astronomical Observatory, Chinese Academy of Sciences for her help and suggestions in writing the paper.

Conflicts of Interest: Authors Jiulong Liu, Jianfeng Sun, Qian Xu, Jiawen Shi and Lidan He were employed by Shanghai Satellite Network Research Institute Co., Ltd. The authors declare no conflicts of interest.

Abbreviations

The following abbreviations are used in this manuscript:

BCRS	Barycentric Celestial Reference System
CDSN	Chinese Deep Space Network
DRO	Distant Retrograde Orbit
ECI	Earth-Centered Inertial coordinate system
EKF	Extended Kalman Filter
GCRS	Geocentric Celestial Reference System
IGSO	Inclined Geosynchronous Orbit
ISL	Inter-Satellite Link
LEO	Low Earth Orbit
LLO	Low Lunar Orbit
LOLA	Lunar Orbiter Laser Altimeter
LRO	Lunar Reconnaissance Orbiter
MEO	Medium Earth Orbit
NRHO	Near-Rectilinear Halo Orbit
POD	Precise Orbit Determination
TDB	Temps Dynamique Barycentrique
TDMA	Time Division Multiple Access
TT	Terrestrial Time
VLBI	Very Long Baseline Interferometry
ΔDOR	Delta Differential One-way Ranging

References

1. Chen, M.; Tang, G.; Cao, J.; Zhang, Y. Precision orbit determination of CE-1 lunar satellite. *Geomat. Inf. Sci. Wuhan Univ.* **2011**, *36*, 212–217. [CrossRef]
2. Li, P.; Hu, X.; Huang, Y.; Wang, G.; Jiang, D.; Zhang, X.; Cao, J.; Xin, N. Orbit determination for Chang'E-2 lunar probe and evaluation of lunar gravity models. *Sci. China Phys. Mech. Astron.* **2012**, *55*, 514–522. [CrossRef]
3. Li, C.; Liu, J.; Ren, X.; Zuo, W.; Tan, X.; Wen, W.; Li, H.; Mu, L.; Su, Y.; Zhang, H.; et al. The Chang'e 3 mission overview. *Space Sci. Rev.* **2015**, *190*, 85–101. [CrossRef]
4. Li, C.; Zuo, W.; Wen, W.; Zeng, X.; Gao, X.; Liu, Y.; Fu, Q.; Zhang, Z.; Su, Y.; Ren, X.; et al. Overview of the Chang'e-4 mission: Opening the frontier of scientific exploration of the lunar far side. *Space Sci. Rev.* **2021**, *217*, 35. [CrossRef]
5. Xiao, L.; Qian, Y.; Wang, Q.; Wang, Q. The Chang'e-5 mission. In *Sample Return Missions*; Elsevier: Amsterdam, The Netherlands, 2021; pp. 195–206. [CrossRef]
6. Liu, H.; Cao, J.; Cheng, X.; Peng, J.; Tang, G. The data processing and analysis for the CE-5T1 GNSS experiment. *Adv. Space Res.* **2017**, *59*, 895–906. [CrossRef]
7. Yue, Z.; Gou, S.; Sun, S.; Yang, W.; Chen, Y.; Wang, Y.; Lin, H.; Di, K.; Lin, Y.; Li, X.; et al. Geological context of the Chang'e-6 landing area and implications for sample analysis. *Innovation* **2024**, *5*, 100633. [CrossRef] [PubMed]
8. Jing, K.; Xie, J.; Hu, G.; Liu, J.; Ma, C.; Wu, S.; Li, K. Orbit Determination and Accuracy Evaluation of Queqiao Relay Satellite for Orbit Maintenance. *J. Deep Space Explor.* **2023**, *10*, 652–658. [CrossRef]
9. Williams, J.G.; Konopliv, A.S.; Boggs, D.H.; Park, R.S.; Yuan, D.-N.; Lemoine, F.G.; Goossens, S.; Mazarico, E.; Nimmo, F.; Weber, R.C.; et al. Lunar interior properties from the GRAIL mission. *J. Geophys. Res. Planets* **2014**, *119*, 1546–1578. [CrossRef]
10. Policastri, L.; Carrico, J.P.; Nickel, C.; Kam, A.; Lebois, R.; Sherman, R. Orbit determination and acquisition for LADEE and LLCD mission operations. In Proceedings of the 25th AAS/AIAA Space Flight Mechanics Meeting, Williamsburg, VA, USA, 15 November 2015.
11. Batcha, A.L.; Williams, J.; Dawn, T.F.; Gutkowski, J.P.; Widner, M.V.; Smallwood, S.L.; Killeen, B.J.; Williams, E.C.; Harpold, R.E. Artemis I trajectory design and optimization. In Proceedings of the 2020 AAS/AIAA Astrodynamics Specialist Conference, South Lake Tahoe, CA, USA, 9–13 August 2020.
12. Gardner, T.; Cheetham, B.; Forsman, A.; Meek, C.; Kayser, E.; Parker, J.; Thompson, M.; Latchu, T.; Rogers, R.; Bryant, B.; et al. Capstone: A cubesat pathfinder for the lunar gateway ecosystem. In Proceedings of the 35th Annual Small Satellite Conference, Virtual, 7–12 August 2021. Available online: https://digitalcommons.usu.edu/smallsat/2021/all2021/142/ (accessed on 25 August 2026).
13. Mazarico, E.; Neumann, G.A.; Barker, M.K.; Goossens, S.; Smith, D.E.; Zuber, M.T. Orbit determination of the Lunar Reconnaissance Orbiter: Status after seven years. *Planet. Space Sci.* **2018**, *162*, 2–19. [CrossRef] [PubMed]
14. Yuan, J.; Huang, Y.; Li, P.; Zhang, Z.; Ma, Y.; Yang, P.; Huang, Y. Orbit determination for Chang'e-6 mission during the lunar orbit phase. *Adv. Space Res.* **2025**, *76*, 4417–4429. [CrossRef]
15. Wang, D.; Xu, T.; Li, M.; Meng, Y.; Gao, W.; Cong, D.; Wang, S.; Shi, Y.; He, B. Lunar navigation satellite system for the South Pole and Earth–Moon space: Constellation design and performance evaluation with integrated BDS. *GPS Solut.* **2025**, *29*, 87. [CrossRef]
16. Liu, L.; Wu, W.-R.; Liu, Y. Design and implementation of Chinese libration point missions. *Sci. China Inf. Sci.* **2023**, *66*, 191201. [CrossRef]
17. Turner, G. Results of long-duration simulation of distant retrograde orbits. *Aerospace* **2016**, *3*, 37. [CrossRef]
18. Zimovan-Spreen, E.M.; Howell, K.C.; Davis, D.C. Dynamical structures nearby NRHOs with applications to transfer design in cislunar space. *J. Astronaut. Sci.* **2022**, *69*, 718–744. [CrossRef]
19. Welch, C.M.; Parker, J.S.; Buxton, C. Mission considerations for transfers to a distant retrograde orbit. *J. Astronaut. Sci.* **2015**, *62*, 101–124. [CrossRef]
20. Sanna, D.; Leonardi, E.M.; De Angelis, G.; Pontani, M. Optimal impulsive orbit transfers from gateway to low lunar orbit. *Aerospace* **2024**, *11*, 460. [CrossRef]
21. Han, Y.; Huang, Y.; Fan, M.; Li, P. Analysis of cislunar DRO orbit determination accuracy using earth-based simulated observations. *J. Deep Space Explor.* **2024**, *11*, 405–413. [CrossRef]
22. Li, S.; Pu, J.; Guo, P.; Wang, W.; Zhang, W. Single-beam differential relative navigation of DRO satellite formation. *J. Deep Space Explor.* **2023**, *10*, 211–219. [CrossRef]
23. Zhou, Y.; Wang, Y.; Huang, W.; Yang, J.; Sun, L. In-orbit performance assessment of BeiDou intersatellite link ranging. *GPS Solut.* **2018**, *22*, 119. [CrossRef]
24. Tang, C.; Hu, X.; Zhou, S.; Liu, L.; Pan, J.; Chen, L.; Guo, R.; Zhu, L.; Hu, G.; Li, X.; et al. Initial results of centralized autonomous orbit determination of the new-generation BDS satellites with inter-satellite link measurements. *J. Geod.* **2018**, *92*, 1155–1169. [CrossRef]

25. Luo, P.; Song, Y.-Z.; Yang, J.; Hu, X.; Tang, C.; Li, K.; Wu, Q. A preliminary result for centralized autonomous orbit determination of gnss constellation and lunar satellite based on inter-satellite link measurements. *GPS Solut.* **2024**, *28*, 173. [CrossRef]
26. Huang, Y.; Yang, P.; Chen, Y.; Li, P.; Zhou, S.; Tang, C.; Hu, X. Orbit determination of a cislunar space probe using Inter-satellite Link data. *Sci. Sin. Phys. Mech. Astron.* **2023**, *53*, 229513. [CrossRef]
27. Chen, S.; Li, S.; Pu, J.; Xu, Y.; Wang, W. Autonomous Orbit Determination of LLO Satellite Using DRO–LLO Links and Lunar Laser Ranging. *Aerospace* **2025**, *12*, 576. [CrossRef]
28. Petit, G.; Luzum, B. (Eds.) *IERS Conventions (2010)*; IERS Technical Note No. 36; Verlag des Bundesamts für Kartographie und Geodäsie: Frankfurt am Main, Germany, 2010.
29. Tang, C.; Hu, X.; Chen, J.; Liu, L.; Zhou, S.; Guo, R.; Li, X.; He, F.; Liu, J.; Yang, J. Orbit determination, clock estimation and performance evaluation of BDS-3 PPP-B2b service. *J. Geod.* **2022**, *96*, 60. [CrossRef]

Disclaimer/Publisher's Note: The statements, opinions and data contained in all publications are solely those of the individual author(s) and contributor(s) and not of MDPI and/or the editor(s). MDPI and/or the editor(s) disclaim responsibility for any injury to people or property resulting from any ideas, methods, instructions or products referred to in the content.